

Ultrafast third-harmonic spectroscopy of single nanoantennas fabricated using helium-ion beam lithography

H. Kollmann^a, M. Esmann^a, S.F. Becker^a, X. Piao^b, C. Huynh^c, L.-O. Kautschor^c, G. Bösker^c, H. Vieker^d, A. Beyer^d, A. Götzhäuser^d, N. Park^b, M. Silies^{a,*}, and C. Lienau^a

^a Institute of Physics, University of Oldenburg, D-26129 Oldenburg, Germany

^b Photonics Systems Laboratory, Seoul National University, Seoul 151-744, Korea

^c Carl Zeiss Microscopy GmbH, D-73447 Oberkochen, Germany

^d Faculty of Physics, Bielefeld University, D-33615 Bielefeld, Germany

*martin.silies@uni-oldenburg.de

ABSTRACT

Metallic nanoantennas are able to spatially localize far-field electromagnetic waves on a few nanometer length scale in the form of surface plasmon excitations¹⁻³. Standard tools for fabricating bowtie and rod antennas with sub-20 nm feature sizes are Electron Beam Lithography or Ga-based Focused Ion Beam (FIB) Milling. These structures, however, often suffer from surface roughness and hence show only a limited optical polarization contrast and therefore a limited electric field localization.

Here, we combine Ga- and He-ion based milling (HIM) for the fabrication of gold bowtie and rod antennas with gap sizes of less than 6 nm combined with a high aspect ratio. Using polarization-sensitive Third-Harmonic (TH) spectroscopy, we compare the nonlinear optical properties of single HIM-antennas with sub-6-nm gaps with those produced by standard Ga-based FIB. We find a pronounced enhancement of the total TH intensity of more than three in comparison to Ga-FIB antennas and a highly improved polarization contrast of the TH intensity of 250:1 for He-ion produced antennas⁴.

These findings combined with Finite-Element Method calculations demonstrate a field enhancement of up to one hundred in the few-nanometer gap of the antenna. This makes He-ion beam milling a highly attractive and promising new tool for the fabrication of plasmonic nanoantennas with few-nanometer feature sizes.

Keywords: Helium-Ion Lithography, Few-nanometer feature sizes, Plasmonic Gold Nanoantennas, Third Harmonic Spectroscopy, Ultrashort Laser Pulses, Diffraction-limited single Antenna Microscopy, Highly confined enhanced electric field

1. INTRODUCTION

Plasmonic Nanostructures are nowadays often used as functional elements to study the interaction between light and single nanometer-sized quantum objects. When, for example, being excited by an external electromagnetic field, their intense evanescent near field can be used to generate femtosecond pulses of electrons⁵ or extreme UV radiation⁶. The concentrated near-field in the surrounding of the nanometer-sized curvatures of the antenna can furthermore be used to image, e.g., single quantum dots⁷. By bringing two or even more of these antennas in close vicinity to each other, the strength of the combined near-field can be further enhanced, forming a so called gap plasmon. This gap plasmon is only present within the confined volume that is formed by the neighboring nanoantennas^{3,8}. Nowadays different bottom-up approaches are commonly used to generate size-optimized particles or even pairs of particles with a few nanometer distances⁹⁻¹¹. On the other hand, top-down fabrication processes such as focused ion beam (FIB) milling¹²⁻¹⁵ or photo resist-based electron beam lithography (EBL)¹⁶⁻²⁰ have made great progress towards the fabrication of structures with feature sizes of down to 10nm. Very recently, He⁺ ion lithography was introduced as a new top-down method to fabricate nanostructures with even smaller feature sizes^{21,22}. In FIB lithography, Ga⁺ ions are typically used for milling. This necessarily limits the resolution to typically more than 10 nm and results in undesired Ga⁺-ion implantation at the interface^{6,13,23}. This effect increases the surface

roughness and modifies the effective dielectric function of the plasmonic antenna. Photo-resist-based Electron-Beam Lithography, on the other hand, can be used to fabricate antennas with gap sizes below 10nm²⁴, however only at very high kinetic energies and by using special types of substrates like SiN membranes and sophisticated electron beam resists.

It is now the aim of this work to introduce a new fabrication technique for plasmonic nanoantennas with unprecedented spatial precision. We propose that a combination of standard Ga⁺-FIB and He⁺-based ion beam lithography (HIL) can fabricate plasmonic antennas with gap sizes as small as 6 nm, significantly smaller than with other techniques. Linear extinction spectroscopy in combination with polarization- and spectrally-resolved nonlinear optical microscopy studies clearly demonstrate that the nonlinear emission - a highly sensitive indicator of local variations in electric field strength - is largely enhanced by field localization within the few-nanometer-sized antenna gap. Finite element method (FEM) simulations of the interaction of light with the bowtie structures strongly support this conclusion. HIL-antennas are found to emit a substantially enhanced third harmonic intensity and show a considerably improved polarization contrast when compared with structures produced by state-of-the-art Ga⁺-FIB.

2. NANOANTENNAS PRODUCED WITH HELIUM-ION LITHOGRAPHY

In a top-down production approach for a plasmonic nanoantenna, a metallic film with typically few tens of nanometer thickness is modified by accelerating and focusing both heavy or light ions, e.g., Gallium or Helium, onto the metal surface. While the heavier ions can be used to remove a large amount of material, this also results in limited precision of milling and an implementation of metallic ions in the modified edge regions of the antenna. Helium ion beam lithography can overcome this problem. As it is illustrated in Figure 1(a), the mass of these ions is a factor of 17 smaller than that of Ga ions. Therefore, their kinetic energy and hence their interactions with the metallic nanostructure is significantly reduced, resulting in an improved milling precision. Monte-Carlo simulations of the penetration paths of He⁺-ions (Figure 1 (b)) and to Ga⁺-ions into a metal furthermore show that He⁺-ions penetrate deeply into the substrate, limiting the interaction of backscattered ions with the material. The interaction zone within the first tens of nanometers is therefore drastically decreased for these lighter ions. This again improves the milling precision even further. Additionally, chemical contamination with the Gallium metallic ions is avoided. However, due to their small masses, the fabrication speed for plasmonic nanostructures is limited when using He⁺-ions.

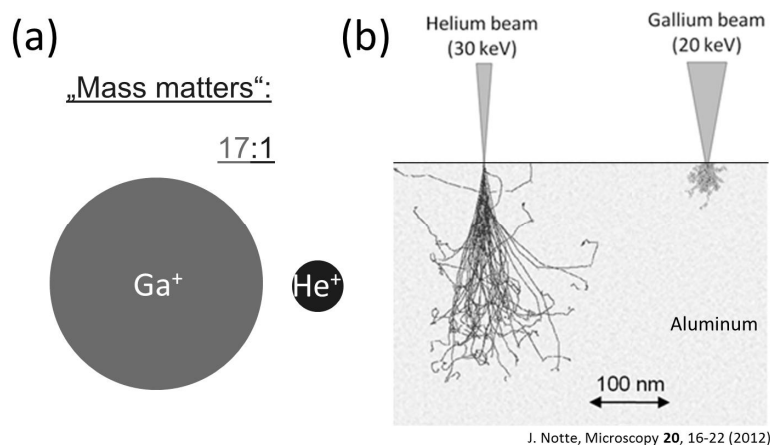


Figure 1(a): Focused ion beam milling techniques typically use heavy-mass ions for fabrication, limiting the fabrication accuracy to more than 10nm. Helium ions with a 17 times smaller mass can now also be used for lithography. (b) Monte-Carlo simulation of the penetration of Ga⁺ and He⁺ ions of comparable kinetic energy into aluminum. The large penetration depth of He⁺ ions leads to a drastically decreased amount of backscattered ions. The interaction volume within the first tens of nanometers is further decreased and the spatial milling precision is increased²⁵ (with permission of J. Notte).

Here, we take advantage of both the higher milling speed of Ga-FIB and the unrivaled milling accuracy of He-FIB to fabricate bowtie nanostructures that consist of two equal-sized triangles with side length of about 260 nm. These structures are compared to bowties that are fabricated with a Ga-FIB production technique alone. In Figure 2, scanning electron images of the antenna fabrication process are shown. Gold films with a thickness of 30 nm with grain sizes of up to 500 nm are produced by electron-beam evaporation and a consecutive flame-annealing process (Fig. 2(a) and (b)). The Ga-beam of a FEI Helios Nanolab 600i Dual Beam is afterwards used to produce arrays of connected antennas with defined antenna dimensions (c). In a second step, a smaller Ga ion current is used to produce antennas with gap sizes of 35nm and 20nm and with radii of curvature of about 12nm. For reasons of comparison, some fused antennas without a gap were produced in addition. Some of these antennas are now used to fabricate bowtie antenna structures with gap sizes of less than 6nm and radii of curvature of 6nm using a Helium ion beam from a Carl Zeiss Orion Plus Microscope. The high quality and excellent sharpness of the boundaries of these antennas is visible in both the top-view SEM image in Fig. 2(g) and the tilted view in Fig. 2(h). In Fig. 2(i), a cross-section of the bowtie antenna from (g) is shown, indicating that the gap is smaller than 6nm. As can be seen in (d) to (g), all antennas only differ slightly in terms of their geometric dimensions.

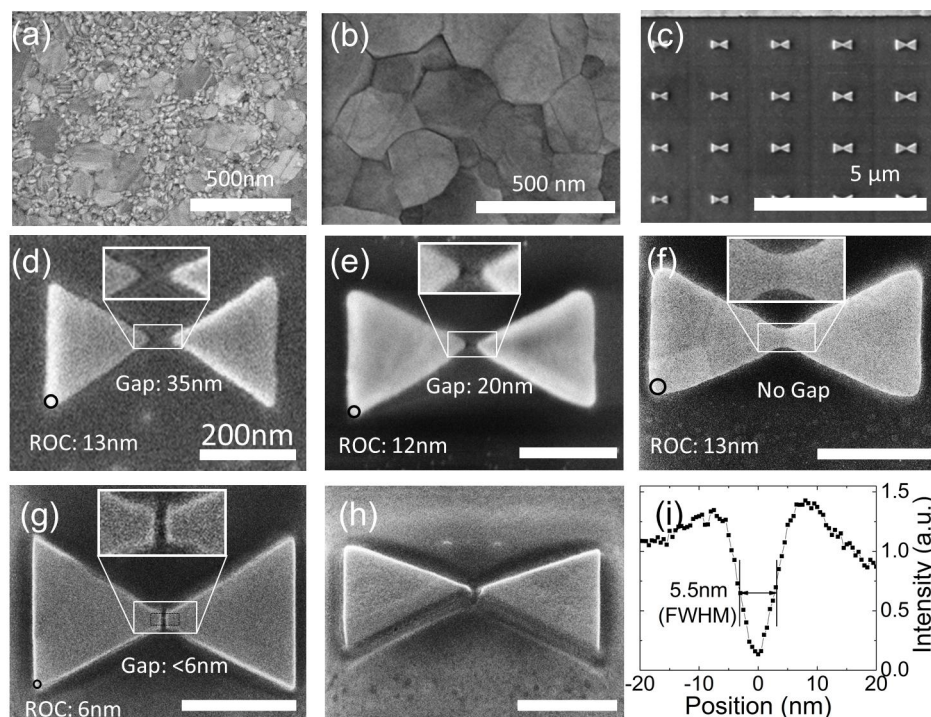


Figure 2 (a)-(h): Scanning electron micrographs of the bowtie production process. (a) 30nm thick polycrystalline gold films are produced in an electron beam physical evaporation process. (b) The film is flame-annealed to increase the grain size from 50 nm to about 500nm. (c) Arrays of connected antennas are produced by a first rough Ga-ion milling process. (d)-(f) In the consecutive fabrication process defined antenna gaps of 35nm and 20nm or antennas with fused triangles are produced. (g) Helium ion lithography is used to mill gaps with sizes of 6nm and radii of curvature of 6nm into the fused triangles. In (h), the excellent aspect ratio of the HIL-produced antenna is shown in a tilted view. (i) Cross-section through the gap region of (g), indicating a gap width of 5.5nm. Scale bars are 200nm unless indicated otherwise.

3. LINEAR OPTICAL SPECTROSCOPY

In a first step, linear extinction measurements of single bowtie antennas with gap sizes of 20 nm fabricated with the Ga⁺- beam and 6 nm fabricated with the He⁺- beam are performed. Additionally, antennas without gaps are analyzed for reasons of comparison. In Fig. 3(a), the experimental set-up of the white-light extinction spectroscopy set-up is shown. Single antennas positioned on a 3D piezo scanner in a confocal microscopy set-up are excited by the light generated by a halogen white light source. A pinhole behind the collecting objective selects the signal of a single antenna. The absorption is measured between 700 nm and 1600 nm in transmission using a monochromator in combination to an InGaAs camera. Representative normalized absorption spectra of the three selected antenna geometries are shown in the upper graph of Fig. 3(b).

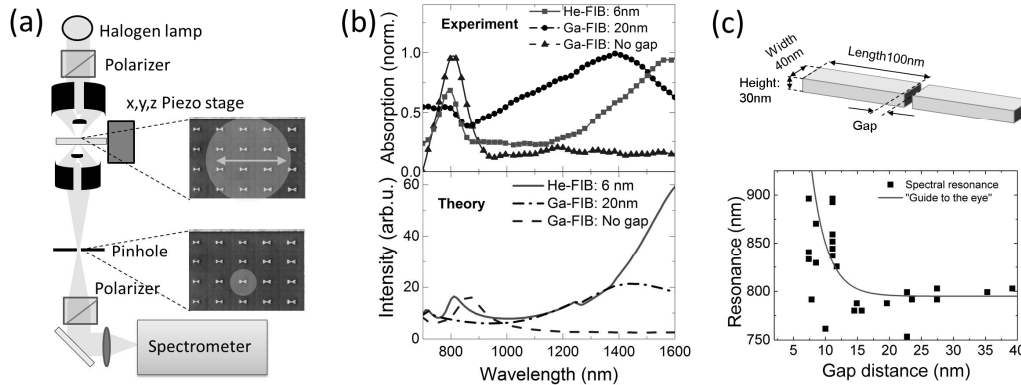


Figure 3 (a): White-light extinction spectroscopy set-up. Linear-polarized light from a halogen lamp is focused to an array of bowtie antennas using a home-built confocal microscope. The extinction spectrum of a single bowtie antenna between 700 nm and 1600 nm is selected using a pinhole and analyzed in a spectrometer. (b) Top: Linear extinction spectra of single bowtie antennas with gap sizes of 6nm (He-FIB, squares); 20nm (Ga-FIB, circles) and an antenna without gap (triangles). Bottom: Simulations of near-field intensity spectra $I(\lambda) = \int |E_x(\lambda, x, y, z = 15nm)|^2 dx \cdot dy$ of the three antenna geometries, recorded at half the antenna height. The calculated energies and spectral widths of the main resonances agree well with experiment. (b) The observed red shift for the bowtie antenna for decreasing gap size is further investigated by a detailed analysis of similar rod antenna pairs with dimensions of 100nm x 40nm x 30nm with varying gap distance. For decreasing gap distance smaller than 15nm, this red-shift becomes visible.

Here, the solid line with squares denotes the absorption spectrum of an antenna with a gap of 6 nm fabricated using Helium ion beam lithography, the dashed line with filled circles represents the absorption spectrum of Ga-FIB antenna with a gap of 20 nm and the dash-dotted line with triangles the absorption spectrum of a fused antenna without gap. In the lower part of Fig.4(b), simulated spatially-integrated near-field distribution spectra $I(\lambda) = \int |E_x(\lambda, x, y, z = 15nm)|^2 dx \cdot dy$ deduced from finite element method (FEM) calculations after excitation with a spatially, homogenous, horizontally-polarized electric field are shown. These spectra are averaged over the field intensities in a plane parallel to the substrate and located at half the antenna height. As can be seen from both graphs, the measured spectra are in convincing agreement with the simulations. Both, the spectral positions of the main resonances and their optical line widths match reasonably well. In particular, the pronounced red shift of the bright dipolar mode of the He⁺-FIB antenna by more than 200 nm compared to the Ga⁺-FIB antenna bowtie with a 20 nm gap can be found in both the experiment and the simulation. To support the observation, that the red-shift and therefore the coupling of the antenna pair becomes stronger for decreasing gap distance, we have additionally analyzed the linear extinction signal of pairs of gold rod antennas with dimensions of 100 x 40 x 30 nm³ (Fig. 3(c)) for different gap sizes, ranging from 40 nm to 6 nm. As can be seen in Fig. 3(c), the main resonance of these antennas increases for decreasing gap size, in agreement with our previous observation for bowtie antennas. This red-shifted main resonance of the bowtie and the rod antennas for decreasing gap sizes reflects the increased coupling of the antenna pair and therefore for the field enhancement in the gap region.

4. THIRD HARMONIC MICROSCOPY OF SINGLE ANTENNAS

In order to study in more detail the optical field enhancement in the bowtie antennas, we now investigate the nonlinear, third harmonic optical response to p-polarized excitation of single bowtie antennas. Third harmonic (TH) microscopy technique has proven itself as a reliable and fast method to study field localization of single or arrays of plasmonic antennas. It is furthermore extremely sensitive to small local field enhancement within the gap of the plasmonic antenna^{17,26-28}. Single bowtie antennas without gap, a gap of 35 nm and 20 nm using a Ga-ion beam and a gap of 6 nm using a He-ion beam are excited with dispersion-compensated, few-cycle laser pulses ranging from 650 nm to 1200 nm, derived from a Ti:Sapphire laser (Fig. 3(a)). These pulses are focused to their diffraction limit onto the antenna by means of an all-reflective Cassegrain objective. While moving the antenna arrays through the focus along the x and y direction the nonlinear emission is collected in reflection and separated from the scattered laser light at the fundamental by a dichroic mirror and analyzed in a monochromator coupled to a liquid-nitrogen cooled, back-illumination deep depletion CCD camera. The incident power and the polarization can be controlled using dispersion-compensated neutral density filters and a half wave plate.

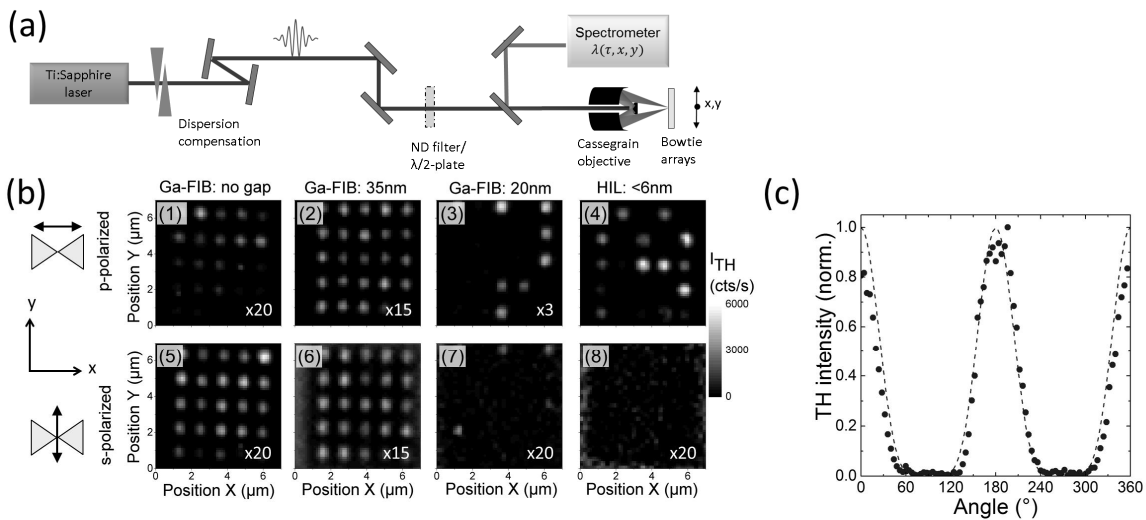


Figure 4 (a): Experimental set-up of the ultrafast nonlinear microscope. Dispersion-balanced, 8-fs laser pulses from a Ti:Sapphire oscillator are focused onto the plasmonic antenna structures using an all-reflective Cassegrain objective. Nonlinear emission from the sample is collected in reflection geometry, dispersed in a spectrometer and detected with a CCD camera.

(b) Third harmonic intensity maps for the four antenna geometries with antennas without gap ((1) and (5)) and gap distances of 35nm ((2) and (6)), 20nm ((3) and (7)), and 6nm ((3) and (8)), for p- and s-polarized excitation. The number in each figure gives the intensity normalization factor in the respective measurement. (c) Polarization-resolved TH intensity of a single bowtie antenna with a gap distance of 6nm. The angle dependence can be reproduced by \cos^6 -function (dashed line), as expected for a TH process.

In Fig. 4(b), spectrally-integrated TH intensity maps for p-polarized (i.e. parallel to the antenna axis, upper row) and for s-polarized light (perpendicular to the antenna, lower row) for the four antenna geometries are shown. The multiplication factor in each TH map denotes an intensity multiplication factor in the respective measurement. While the TH signal for the antennas without gap is low and is independent of the incident polarization of the laser light, the signal increases for decreasing gap sizes for p-polarized light, as can be seen by the decreasing multiplication factor. Furthermore, the signal nearly vanishes for small gap distances of 20nm and of 6nm for s-polarized excitation. For 6-nm gaps, the signal is e.g. by more than an order of magnitude higher than for antennas with gap distances of 35 nm revealing the improved ability of the antennas with small gaps to localize light. While now detecting the TH intensity of a single antenna with a gap of 6 nm, we now vary the incident polarization from 0° to 360° (filled circles in Fig. 4(c)). The measured TH intensity is nicely reproduced by a \cos^6 -angle dependence, indicated by the dashed line in (c), as expected for a third harmonic process. Again, the TH signal completely disappears for s-polarized light with a polarization contrast of about 250:1. This indicates an excellent surface quality of those antennas and efficient electric field confinement within the nm-sized gap region.

5. FEM SIMULATIONS

We finally compare our experimental findings with three-dimensional finite-element method calculations of the optical near-field distribution around the bowtie-antennas after excitation with a p-polarized (along the x-direction) plane-wave optical pulse. The pulse spectrum matches that of the experimentally used ultrashort laser pulses. In Fig. 5, the enhancement of the dominant electric field component along the x-direction, $|E_x|/|E_0|$, is shown for the three of the four investigated geometries at mid-height of the structure, i.e. at $z = 15\text{nm}$. The inset of each Figure shows a magnification of the gap region with a modified enhancement scale ranging from $|E_x|/|E_0| = 0$ to 100. As can be seen in the image, the enhancement of the electric field within the intersection of the two triangles is only slightly visible for the structure without gap and increases for decreasing gap size. It reaches a value of more than 100 for the bowtie with a gap of 6 nm and remains essentially constant with the gap region. Given the excellent aspect ratio demonstrated in Figure 1c, the bowtie antenna essentially acts as a nanoscopic parallel plate capacitor with sidewall areas of approximately $30 \times 30 \text{ nm}^2$ and a separation of only 6 nm. This makes it a particularly attractive nanocavity for localizing electromagnetic fields with well-defined polarization properties to nanometric volumes and to explore their enhanced coupling to nanoemitters.

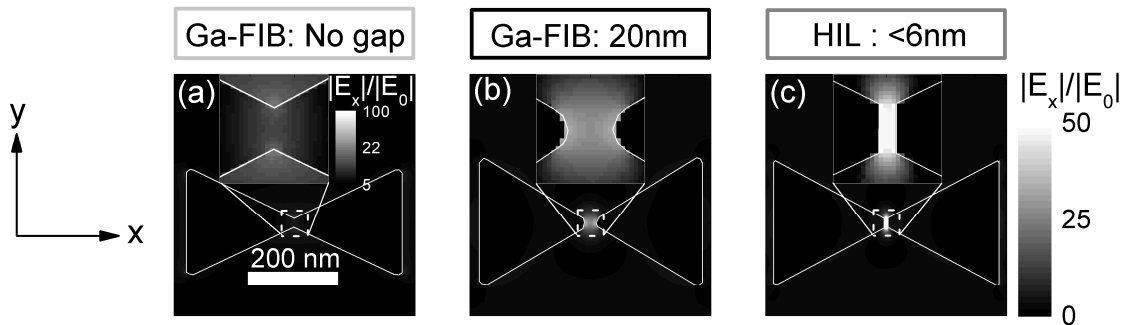


Figure 5 (a): Finite element method calculations of the electric near field enhancement $|E_x|/|E_0|$ after excitation with optical pulse polarized along the x-direction. The pulse spectra match those used in experiment. (a) Ga-FIB antenna without gap, (b) Ga-FIB antenna with a gap of 20nm and (c) a He-FIB antenna with a gap of less than 6 nm. The insets in the Figures show a zoom into the gap region of the antenna with a two times larger enhancement scale.

6. CONCLUSION

Taken together, we were able, by using a combination of Ga^+ - and He^+ - ion beam milling, to fabricate plasmonic nanostructures with excellent few-nanometer milling precision. Gold bowtie antennas with gap distances as small as 6 nm could be fabricated, significantly smaller than by using Ga^+ - ion beam milling alone. Here, structures with gap distances of about 20 nm could be fabricated. The linear response of these structures has been analyzed in a linear extinction spectroscopy set-up. The measured red-shift of the main resonance for the structures with 6-nm gaps was taken as a signature of the pronounced light localization in the antenna gaps. The third harmonic response of those antennas was tested in a nonlinear confocal microscope setup. We found an increase in TH intensity by more than a factor of 3 compared to the best bowties antennas that were fabricated by Ga-FIB alone. Finite element method calculations support our experimental findings, and suggest that our structures show a remarkably high field enhancement within the nanometer gap region. This new technique, combining Gallium and Helium ion beam milling, can therefore pave the way towards plasmonics with nanometer precision.

REFERENCES

- [1] Bharadwaj, P., Deutsch, B. & Novotny, L. Optical Antennas. *Adv. Opt. Photon.* **1**, 438-483, doi:10.1364/aop.1.000438 (2009).
- [2] Schuck, P. J., Fromm, D. P., Moerner, W. E., Sundaramurthy, A. & Kino, G. QMH1 (Optical Society of America).

- [3] Siegfried, T., Ekinici, Y., Martin, O. J. F. & Sigg, H. Gap Plasmons and Near-Field Enhancement in Closely Packed Sub-10 nm Gap Resonators. *Nano Letters* **13**, 5449-5453, doi:10.1021/nl403030g (2013).
- [4] Kollmann, H. *et al.* Toward Plasmonics with Nanometer Precision: Nonlinear Optics of Helium-Ion Milled Gold Nanoantennas. *Nano Letters* **14**, 4778-4784, doi:10.1021/nl5019589 (2014).
- [5] Ropers, C., Solli, D. R., Schulz, C. P., Lienau, C. & Elsaesser, T. Localized Multiphoton Emission of Femtosecond Electron Pulses from Metal Nanotips. *Physical Review Letters* **98**, 043907 (2007).
- [6] Sivilis, M., Duwe, M., Abel, B. & Ropers, C. Extreme-ultraviolet light generation in plasmonic nanostructures. *Nat Phys* **9**, 304-309, doi:10.1038/nphys2590 (2013).
- [7] Javad, N. F. *et al.* Bow-tie optical antenna probes for single-emitter scanning near-field optical microscopy. *Nanotechnology* **18**, 125506 (2007).
- [8] Schuller, J. A. *et al.* Plasmonics for extreme light concentration and manipulation. *Nat Mater* **9**, 193-204 (2010).
- [9] Yu, Chang, S.-S., Lee, C.-L. & Wang, C. R. C. Gold Nanorods: Electrochemical Synthesis and Optical Properties. *The Journal of Physical Chemistry B* **101**, 6661-6664, doi:10.1021/jp971656q (1997).
- [10] Sun, Y. & Xia, Y. Shape-Controlled Synthesis of Gold and Silver Nanoparticles. *Science* **298**, 2176-2179, doi:10.1126/science.1077229 (2002).
- [11] Gole, A. & Murphy, C. J. Seed-Mediated Synthesis of Gold Nanorods: Role of the Size and Nature of the Seed. *Chemistry of Materials* **16**, 3633-3640, doi:10.1021/cm0492336 (2004).
- [12] Farahani, J. N., Pohl, D. W., Eisler, H. J. & Hecht, B. Single Quantum Dot Coupled to a Scanning Optical Antenna: A Tunable Superemitter. *Physical Review Letters* **95**, 017402 (2005).
- [13] Huang, J.-S. *et al.* Mode Imaging and Selection in Strongly Coupled Nanoantennas. *Nano Letters* **10**, 2105-2110, doi:10.1021/nl100614p (2010).
- [14] Kim, S. *et al.* High-harmonic generation by resonant plasmon field enhancement. *Nature* **453**, 757-760 (2008).
- [15] Sivilis, M., Duwe, M., Abel, B. & Ropers, C. Nanostructure-enhanced atomic line emission. *Nature* **485**, E1-E3 (2012).
- [16] Hanke, T. *et al.* Tailoring Spatiotemporal Light Confinement in Single Plasmonic Nanoantennas. *Nano Letters* **12**, 992-996, doi:10.1021/nl2041047 (2012).
- [17] Hanke, T. *et al.* Efficient Nonlinear Light Emission of Single Gold Optical Antennas Driven by Few-Cycle Near-Infrared Pulses. *Physical Review Letters* **103**, 257404 (2009).
- [18] Muskens, O. L., Giannini, V., Sánchez-Gil, J. A. & Gómez Rivas, J. Strong Enhancement of the Radiative Decay Rate of Emitters by Single Plasmonic Nanoantennas. *Nano Letters* **7**, 2871-2875, doi:10.1021/nl0715847 (2007).
- [19] Koh, A. L., Fernández-Domínguez, A. I., McComb, D. W., Maier, S. A. & Yang, J. K. W. High-Resolution Mapping of Electron-Beam-Excited Plasmon Modes in Lithographically Defined Gold Nanostructures. *Nano Letters* **11**, 1323-1330, doi:10.1021/nl104410t (2011).
- [20] Schlather, A. E., Large, N., Urban, A. S., Nordlander, P. & Halas, N. J. Near-Field Mediated Plexcitonic Coupling and Giant Rabi Splitting in Individual Metallic Dimers. *Nano Letters* **13**, 3281-3286, doi:10.1021/nl4014887 (2013).
- [21] Wang, Y. *et al.* Ultrafast Nonlinear Control of Progressively Loaded, Single Plasmonic Nanoantennas Fabricated Using Helium Ion Milling. *Nano Letters* **13**, 5647-5653, doi:10.1021/nl403316z (2013).
- [22] Bell, D. C., Lemme, M. C., Stern, L. A., Williams, J. R. & Marcus, C. M. Precision cutting and patterning of graphene with helium ions. *Nanotechnology* **20**, 455301 (2009).
- [23] Mühlischlegel, P., Eisler, H. J., Martin, O. J. F., Hecht, B. & Pohl, D. W. Resonant Optical Antennas. *Science* **308**, 1607-1609 (2005).
- [24] Duan, H., Fernández-Domínguez, A. I., Bosman, M., Maier, S. A. & Yang, J. K. W. Nanoplasmonics: Classical down to the Nanometer Scale. *Nano Letters* **12**, 1683-1689, doi:10.1021/nl3001309 (2012).
- [25] Notte, J. A. Charged Particle Microscopy: Why Mass Matters. *Microscopy Today* **20**, 16-22, doi:doi:10.1017/S1551929512000715 (2012).
- [26] Kauranen, M. & Zayats, A. V. Nonlinear plasmonics. *Nat Photon* **6**, 737-748 (2012).
- [27] Hentschel, M., Utikal, T., Giessen, H. & Lippitz, M. Quantitative Modeling of the Third Harmonic Emission Spectrum of Plasmonic Nanoantennas. *Nano Letters* **12**, 3778-3782, doi:10.1021/nl301686x (2012).

- [28] Metzger, B. *et al.* Doubling the Efficiency of Third Harmonic Generation by Positioning ITO Nanocrystals into the Hot-Spot of Plasmonic Gap-Antennas. *Nano Letters* **14**, 2867-2872, doi:10.1021/nl500913t (2014).